Pergamon

Int. J. Heat Mass Transfer. Vol. 39, No. 5, pp. 1081–1091, 1996

0017-9310/96 $15.00+0.00

0017-9310(95)00185-9

Chaotic behavior and heat transfer performance of the natural convection around a hot horizontal cylinder affected by a flat ceiling

H. KOIZUMI and I. HOSOKAWA

Department of Mechanical and Control Engineering, University of Electro-Communications, Chofu, Tokyo 182, Japan

(*Received* 10 *January* 1995 *and in final form* 4 *April* 1995)

Abstract—This study aims to reveal the effect of a flat ceiling on the flow and heat transfer performance around an isothermally heated horizontal cylinder. Experiments are performed with air at Rayleigh numbers ranging from 4.8×10^4 to 1.0×10^7. We show three types of flow patterns depending on Rayleigh number Ra, dimensionless distance H/D between the ceiling and the cylinder, and the temperature condition of the ceiling: three-dimensional unsteady flow in which the flow along the cylinder separates on its upper surface, two-dimensional steady flow, and oscillatory flow. It is shown that the three-dimensional unsteady flow is chaotic, by calculation of a set of Liapunov exponents and the Liapunov dimension from the observed time series of both heat flow and fluid temperature sensors. The oscillatory flow can be also shown to be chaotic.

1. INTRODUCTION

The flow and heat transfer performance of the natural convection around a horizontal cylinder affected by a wall are extremely different from those suspended in an infinite fluid medium [1, 2]. To reveal the change of those characteristics affected by a wall is important in relation to the cooling of electronic devices from the industrial engineering standpoint. As for the natural convection which is similar to this flow system, not a few works have been performed with respect to the effect of the wall on the time-averaged local Nusselt number around a cylinder placed in a finite vessel experimentally [2] and with respect to convective flow patterns in horizontal cylindrical annuli enclosed in heated inner and cooled outer cylinder experimentally and numerically [3–5]. Powe *et al.* [3] investigated the natural convective flow of air between horizontal concentric annuli and categorized flow patterns against Grashof number and the inverse relative gap width experimentally. They showed that at relatively high Grashof numbers three different convective flow patterns were produced as a function of the gap width: unsteady two-dimensional (2D) flow consisting of one or more pairs of small, counter-rotating cells in the upper gap region, oscillatory flow characterized by a 3D spiral motion in the upper portion of the annulus, and 2D unsteady flow characterized by oscillations of the crescent-shaped flow pattern. Takata *et al.* [4] performed a numerical and experimental work on the 3D flow and heat transfer performance in an inclined cylindrical annulus (including the horizontal case) using the steady 3D Boussinesq equations to examine the flow structure and temperature distributions, Nusselt numbers, and effect of inclination on them. Also, Rao *et al.* [5] performed the calculation on the same flow system as Powe *et al.* [3] over a wide range of Rayleigh number and aspect ratio using the unsteady 2D and steady 3D Boussinesq equations. They obtained the general trend presented by Powe *et al.* [3] except for an oscillatory flow in the case of a wide annulus. But there has been no work of clarifying both the instantaneous and time-averaged heat transfer performances around a cylinder affected by an infinite flat ceiling. Furthermore, to reveal the difference of the flow and heat transfer performance between the concentric annuli and this flow system is interesting from the view point of basic heat transfer science.

Recently, there is an idea to submerge a large amount of CO_2, which is a major cause of the global warming, in the deep sea [6]. This idea is that we gather gaseous CO_2 from fossil fuel power plants, compress it into liquid, and then mix it with water to produce clustered CO_2 like sherbet which is a very stable substance. Clustered CO_2 is transported into the bottom of the deep sea by a pipe line and it is pooled in the bottom of a ravine. It is necessary to keep clustered CO_2 for a long period in the deep sea, but there is an anxiety that unsteady strong vortices around a transport pipe enhance convective diffusion of clustered CO_2 in the region near the pipe outlet [7]. The flow and heat transfer performance around a cold horizontal cylinder placed near the bottom of the sea can be understood by the natural convective flow around a hot horizontal cylinder placed near a flat ceiling (by reversing both the vertical axis and temperature).

This research aims to reveal the effect of the flat ceiling on the flow and heat transfer performance

NOMENCLATURE

D	diameter of the cylinder
D_{KY}	Liapunov dimension (or Kaplan–Yorke dimension)
d_m	embedding dimension
H	distance between the ceiling and the cylinder
l	distance between the two thermocouples (Fig. 6)
Nu	time-averaged local Nusselt number
Nu'	fluctuation intensity of local Nusselt number
Nu^*	normalized time-averaged local Nusselt number, Nu/Nu_0 (Nu_0 is the value at the lower stagnation point of the cylinder under the conductive ceiling for $Ra = 1.3 \times 10^6$ and $H/D = 1.0$)
Ra	Rayleigh number, $g\beta(T_{cylinder} - T_{ceiling})D^3/\alpha\nu$
Pr	Prandtl number, ν/α
$R(l)$	cross-correlation of fluid temperature
$T_{ceiling}$	temperature of the ceiling
$T_{cylinder}$	temperature of the cylinder
$\overline{T_f^*}$	time-averaged temperature of fluid, $(\overline{T_f} - T_{ceiling})/(T_{cylinder} - T_{ceiling})$

Physical properties are estimated at the mean temperature $(T_{ceiling} + T_{cylinder})/2$.

Greek symbols

α	thermal diffusivity of fluid
β	coefficient of thermal expansion
Θ	angle, zero is upward vertical, positive counter-clockwise on right half of the cylinder, $0° \leqslant \Theta \leqslant 180°$, (Fig. 1)
λ_i	Liapunov exponent ($i = 1, \ldots, d_m$)
ν	kinetic viscosity of fluid.

around an isothermally heated horizontal cylinder. Experiments are performed with air at Rayleigh numbers below 1.0×10^7, at which the flow along the cylinder suspended in an infinite fluid medium is clearly steady. If the possibly produced unsteady flow is chaotic, a large convective mixing effect may be produced. So we here try to investigate the occurrence of such unsteady flows from the standpoint of chaos.

2. EXPERIMENTAL APPARATUS AND PROCEDURE

2.1. *Experimental apparatus*

Figure 1 shows a schematic view of the experimental apparatus. We use seven copper test cylinders which are 560 mm in length and 3.0 mm in thickness, but with different diameters: 25.4 mm, 38.1 mm, 50.8 mm, 63.5 mm, 76.2 mm, 114.3 mm (only in this case, 5.0 mm in thickness) and 152.4 mm. A 10 μm thick stainless steel foil is pasted onto another cylinder inside the test cylinder. Then the foil is electrically heated by a constant direct current. The surface temperature is kept uniform and constant within 1 K except at both 80 mm long end parts of the cylinder. The temperature difference between the ceiling and the cylinder is set as about 40 K. In order to protect the flow along the cylinder from disturbances, the cylinder is placed in a vessel having dimensions of $1000 \times 600 \times 1200$ mm^3 as shown in Fig. 1. Both sidewall and floor are made of a transparent acryl sheet 8 mm thick. Two different kinds of ceilings are used for clarifying the effect of the temperature condition of the ceiling on the flow and heat transfer performance around the cylinder. The conductive ceiling is made of an aluminum sheet 8 mm thick and cooled by water, so that its surface temperature is kept constant. The adiabatic ceiling is made of a foam glass sheet 20 mm thick, and its surface temperature is uniform except near the heated cylinder. When H/D is small, it is several degrees higher near the heated cylinder because the removal of heat is dependent only on the natural convection through the ceiling. In both cases, the temperature difference between the acryl sheet sidewalls and the ceiling is within about 2 K and kept constant at room temperature. The working medium is air ($Pr = 0.71$) and Rayleigh number is changed by the cylinder diameter D. The experiment is performed for different distances between the ceiling and the cylinder under two temperature conditions of the ceiling (conductive and adiabatic) at Rayleigh numbers ranging from 4.8×10^4 to 1.0×10^7.

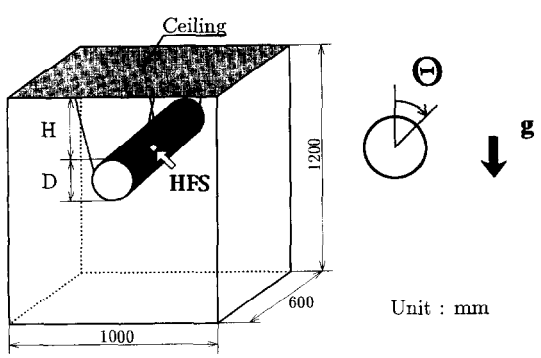

Fig. 1. Schematic view of the experimental apparatus.

2.2. *Nusselt number*

A heat flow sensor (abbreviated as HFS; thickness is 75 μm, sensing area is 1.5×4 mm^2 and response time is about 0.02 s) is pasted on the cylinder surface in the central part of the whole axial length and its output is amplified by 100 000 times. We obtain the

time-averaged values, limits and intensity of fluctuations of the instantaneous local Nusselt number Nu^* from its amplified output using a workstation, normalized by the reproducible local value Nu_0 for $Ra = 1.3 \times 10^6$ at the lower stagnation point of the same cylinder ($D = 76.2$ mm and $\Theta = 180°$) under the conductive ceiling in which the value had no fluctuation at $H/D = 1.0$ in region II. Nu_0 is almost the same value at the lower point of the cylinder suspended in an infinite fluid medium [1, 8] as mentioned in Section 3.2, so that the absolute value of the local Nusselt number, Nu can be calculated from the normalized local Nusselt number Nu^* ($= Nu/Nu_0$) shown in Figs. 4 and 5, if necessary. This technique replaces the usual calibration process of HFS. The sensing position is changed by rotating the cylinder. The space resolution of the sensor is about 2.3° around the cylinder when the outer diameter of the cylinder is 76.2 mm.

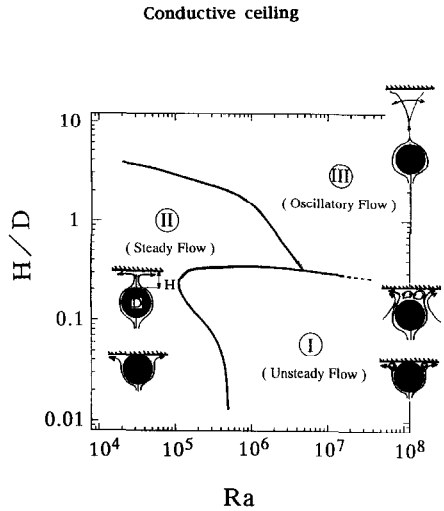

Fig. 2. Flow pattern.

2.3. *Liapunov exponents*

In order to clarify the unsteady characteristics, an instantaneous flow visualization experiment is conducted using incense smoke. Furthermore, we obtain the cross-correlation using two copper–constantan thermocouples of 50 μm diameter (abbreviated as TC and response time is about 0.13 s) placed l mm apart along the axial direction of the cylinder ($\Theta = 0°$) in the midposition between the conductive ceiling and the cylinder when Ra is 1.3×10^6 and H/D is 0.2 in region I of Fig. 2. The cross-correlation is defined as

$$R(l) = \max_{\tau} \{|R_{12}(\tau)/\sqrt{[R_{11}(0)R_{22}(0)]}|\},$$

$$R_{12}(\tau) = \lim_{0 \to \infty} \frac{1}{t_0} \int_0^{t_0} T_1(t) T_2(t+\tau)\, \mathrm{d}t.$$

We obtain the power spectrum and Liapunov exponents λ_i ($i = 1, \ldots, d_m$) from the time-series of HFS or TC. The Liapunov exponents λ_i represent the time-development of the displacement vector between two very adjacent points in the phase space. The exponents can be calculated by the method proposed by Sano and Sawada [9]. When one or more positive exponents are obtained, the flow may be characterized as chaotic with the magnitude of the exponents indicating the time scale for predictability. From a time series of a single variable of the sensor output an attractor is reconstructed in a d_m-dimensional phase space, and then we obtain the Liapunov exponents λ_i by the orbits of points evolving in time τ_{dev}. Also we calculate from these exponents the Liapunov dimension D_{KY} which shows complexity of unsteady flow [10]. The program in this study was tested using the well-known Lorenz model with the same parameters as Sano *et al.* [9] for $d_m = 3$. (For details see [11].)

We sample 131 072 data points from a time-series of HFS or TC by using the a.d. converter with 16 bit resolution and sampling time $\Delta\tau$ is set to 0.01953 s in this experiment. Delay time τ_{del} is chosen as the lag time at which the autocorrelation function of the time series falls to nearly zero. All calculations are carried out on a SUN SPARK 2 workstation.

3. RESULTS AND DISCUSSIONS

3.1. *Flow pattern and visualization*

We consider that the ceiling is infinite in this flow system, so that the geometrical relation between the ceiling and the cylinder becomes similar figures only dependent on dimensionless distance H/D. Therefore, both flow and heat transfer fields are described through Rayleigh number Ra, Prandtl number Pr (0.71 for air), H/D and the temperature condition of the ceiling.

Figure 2 shows the categorization of flow patterns which depend on Ra and H/D in the case of conductive ceiling. Three types of flow patterns are observed: 3D unsteady flow in region I in which the flow along the cylinder separates on its surface, 2D steady flow in region II, and oscillatory flow in region III. Figure 3 shows instantaneous flow visualization photos for $Ra = 1.3 \times 10^6$ in each region of Fig. 2. Figure 3(a) is a photo taken from the axial direction for $H/D = 0.05$ in region I. Figure 3(b1) is from the axial direction and Fig. 3(b2) from the lateral direction for $H/D = 0.2$ in region I. Figure 3(c) is a photo for $H/D = 0.4$ in region II and Fig. 3(d) for $H/D = 2.3$ in region III from the axial direction, respectively.

In region I, the velocity along the cylinder is reduced severely by the ceiling, and then the flow separates on the upper surface of the cylinder and gets unsteady. We illustrate the flow patterns along the cylinder schematically for both cases of $H/D = 0.2$ and 0.05 in Fig. 2. For $Ra = 1.3 \times 10^6$ and $H/D = 0.05$ [Fig. 3(a)], the flow along the cylinder separates around $\Theta = 60°$ from the upper point ($\Theta = 0°$) and shows an unsteady behavior in the region of $\Theta = 20° \sim 60°$. The rolls having axis in the axial direction of the cylinder are

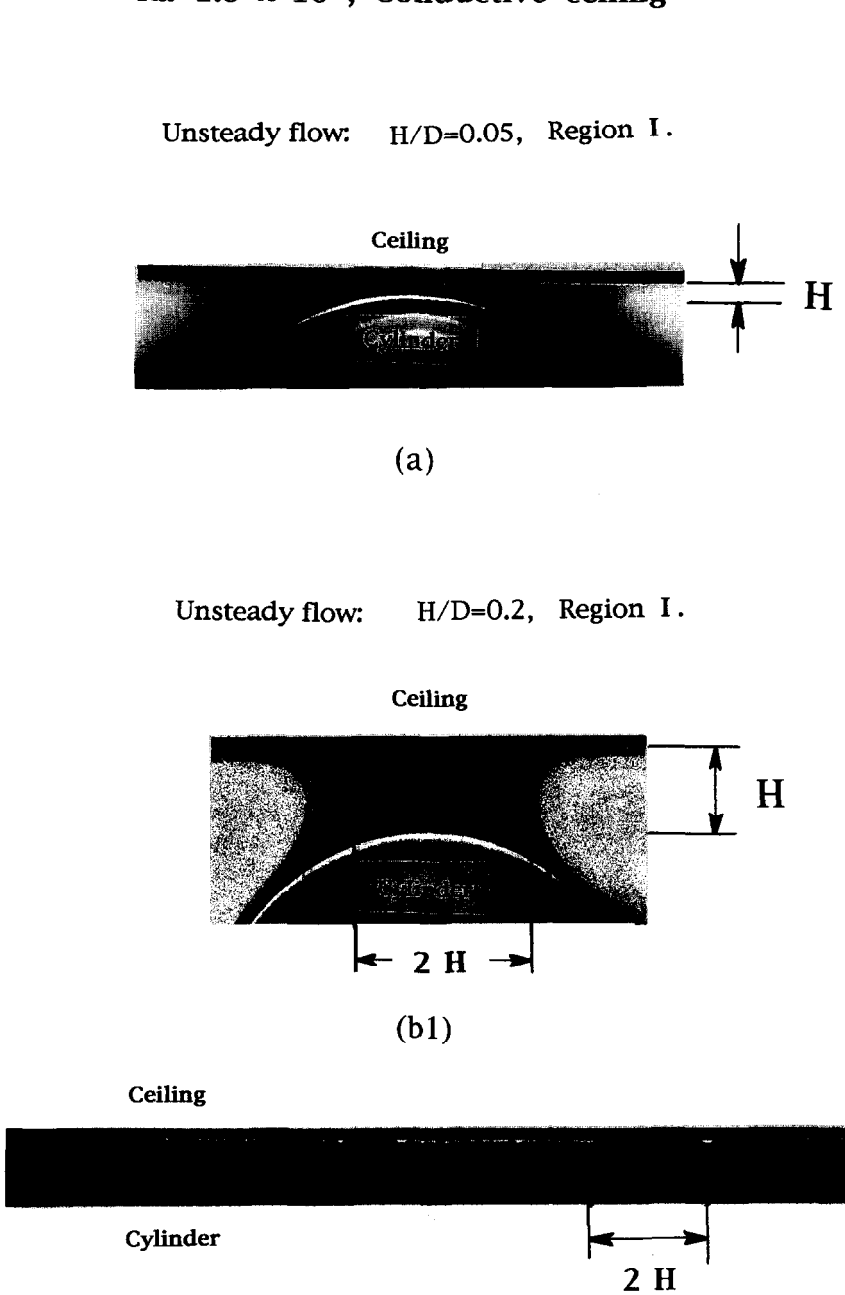

Fig. 3. Photo instantaneous flow visualization: (a) axial direction ($H/D = 0.05$); (b1) axial direction ($H/D = 0.2$); (b2) lateral direction ($H/D = 0.2$); (c) axial direction ($H/D = 0.4$) and (d) axial direction ($H/D = 2.3$).

Steady flow: H/D=0.4, Region II

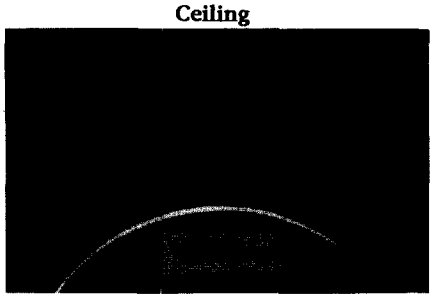

(c)

Oscillatory flow: H/D=2.3, Region III

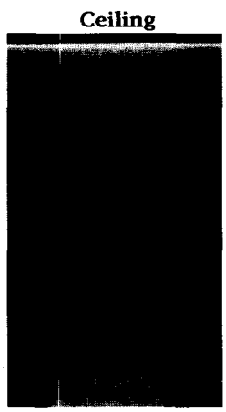

(d)

Fig. 3—*continued.*

observed to produce asymmetrically and oscillate slightly in the wedge-shaped narrow region between the ceiling and the cylinder. For $Ra = 1.3 \times 10^6$ and $H/D = 0.2$, a pair of rolls having an axis in the axial direction and the size of about 2 H are predominantly observed to oscillate slightly [Fig. 3(b1)], and occasionally similar rolls but having an axis in the lateral direction and other smaller vortical structures appear to move irregularly [Fig. 3(b2)]. These vortices have the wavelength, which is close to about 2.016 H, that of unstable lowest mode in the critical flow with Rayleigh–Bénard convection in a layer of infinite horizontal extent with rigid–rigid boundaries [12]. These unsteady 3D flows are extremely different from the unsteady, 2D flow between concentric cylinders which consists of one or more pairs of small, counter-rotating cells in the upper gap region [3]. When the Rayleigh number is below about 1.0×10^5, these unsteady flows do not appear even if H/D is small.

In region II, the separation point on the upper cylinder surface is almost fixed and the flow is 2D. We illustrate the flow patterns along the cylinder schematically for both cases of $H/D = 0.4$ and 0.05 in Fig. 2. When H/D is relatively large, the fluid flows up towards the upper point ($\Theta = 0°$) along the cylinder and then separates from the cylinder surface to ascend in the vertical direction. After the ascending flow stagnates at the ceiling almost at right angles, the flow is divided and flows along the ceiling.

In region III, the stable flow along the cylinder separates near the upper point ($\Theta = 0°$) and ascends in the vertical direction. The ascending flow just near the cylinder is almost 2D but its plume far from the cylinder begins to oscillate extensively from side to side. We illustrate the flow pattern along the cylinder schematically in Fig. 2. This oscillatory flow is 3D and its three-dimensionality becomes much stronger when both Rayleigh number and the distance between the ceiling and the cylinder become larger.

We have performed the experiment to check the reliability of the result obtained in Fig. 2 by changing the temperature difference between the ceiling and the cylinder within 10–80 K in the case of conductive ceiling with the cylinder diameter of 76.2 mm. From this result, we confirm that the categorization of flow patterns shown in Fig. 2 holds true for the Rayleigh numbers ranging from 3.0×10^5 to 3.0×10^6.

3.2. *Nusselt number*

Figure 4 shows the instantaneous, time-averaged local Nusselt number Nu^* and its fluctuation intensity around the cylinder when Ra is 1.3×10^6 in the case of both conductive and adiabatic ceilings in region I of Fig. 2. Figure 4(a) is the result for $H/D = 0.05$ and Fig. 4(b) for $H/D = 0.2$. The circles indicate the normalized time-averaged local Nusselt number Nu^*. White marks indicate the results for conductive ceiling and black ones for adiabatic ceiling. The spline curve which is indicated by a solid line is for the conductive ceiling and a dotted line for adiabatic ceiling, respectively. The error bars show the limits of fluctuation of its instantaneous Nusselt number. The dot-and-dash line shows Nu^* of the steady flow along the cylinder for the conductive ceiling in region II of Fig. 2. The histogram shows the fluctuation intensity of local Nusselt number $\sqrt{[(Nu')^2]}/Nu_0$. The radiation effect is included in this experiment which is supposed to be about 5–9% of total Nusselt number for the adiabatic ceiling made of foam glass. The radiation effect is less important for the conductive ceiling made of an aluminum sheet.

Nu^* decreases gradually from the lower point ($\Theta = 180°$) as the boundary layer develops along the cylinder, but heat transfer performances near the

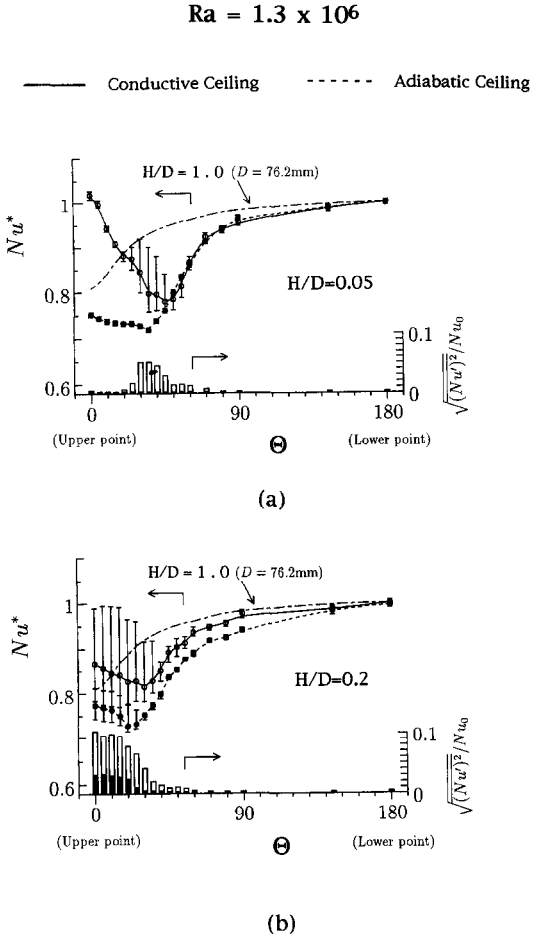

Fig. 4. Nusselt number in region I at $Ra = 1.3 \times 10^6$: (a) $H/D = 0.05$ and (b) $H/D = 0.2$.

upper surface are extremely different in these two cases. In the case of $H/D = 0.05$, the flow along the cylinder for the case of conductive ceiling separates near $\Theta = 60°$ and the fluctuation intensity increases to 2–5% in the region of $\Theta = 20$–$60°$, while for the case of adiabatic ceiling it is below 0.3% all around the cylinder and the separation point is almost fixed. This fluctuation must be responsible for the stability of the flow along the ceiling. Since for the case of conductive ceiling the density decreases in the downward direction and the flow along the ceiling becomes unstable, then this unstable flow enlarges the fluctuation near the separation point. For the case of adiabatic ceiling, the flow is stable and scarcely shows fluctuation around the cylinder. In the case of a higher Rayleigh number, $Ra = 1.0 \times 10^7$, and $H/D = 0.05$, there is some fluctuation around the cylinder for both conductive and adiabatic ceiling. The fluctuation intensity for the adiabatic ceiling is about one-half that for the conductive ceiling.

In the case of $H/D = 0.2$ in Fig. 4(b) the fluctuation intensity increases rapidly from about $\Theta = 40°$ for the case of conductive ceiling and from about $\Theta = 25°$ for the adiabatic ceiling. Then the 3D vortices are observed to fluctuate between the ceiling and the cylinder as is shown in Figs. 3(b1) and (b2). The fluctuation intensity for the case of conductive ceiling is about 2.5 times larger than that for the case of the adiabatic ceiling.

We investigated the effect of the vessel size as shown in Fig. 1 on the heat transfer performance around the cylinder for the case of conductive ceiling. The results shown in Fig. 4(b) do not change even if the vessel size has changed from 1000 mm to 600 mm in width or from 600 mm to 350 mm in depth (axial direction of the cylinder) independently.

Figure 5 shows the instantaneous, time-averaged local Nusselt number Nu^* and its fluctuation intensity around the cylinder at $Ra = 1.3 \times 10^6$ for the conductive ceiling for both the steady flow in region II and the oscillatory flow in region III of Fig. 2. The symbols used in the figure are the same as in Fig. 4. The spline curve indicated by a dot-and-dash line shows Nu^* of the steady flow of $H/D = 1.0$ and a solid line shows Nu^* of the oscillatory flow of $H/D = 2.3$.

Nu^* shows almost the same distributions in these two cases and it decreases gradually from the lower point ($\Theta = 180°$) as the boundary layer develops along the cylinder. Furthermore, the flows passing very near the cylinder are stable for both cases and the fluctuation intensity there is below about 0.3% all the way along the cylinder. That is, the swaying motion of the ascending flow far from the cylinder does not affect the heat transfer performance around the cylinder in the case of $H/D = 2.3$.

We performed the experiment by removing the ceiling of the vessel as is shown in Fig. 1, which simulated the flow along the cylinder suspended in an infinite fluid medium ($H/D \sim \infty$). In this case, we obtained the relative time-averaged local Nusselt number Nu^* ($Nu^* = 1$) at the lower point of the cylinder ($\Theta = 180°$) from HFS. This value, $Nu^* = 1$, is in good agreement with the result which is shown in Fig. 5 for the conductive ceiling and $H/D = 1.0$ in region II within about 5%. Therefore, the local Nusselt number Nu_0 in the lower point of the cylinder used for normalization in this experiment must agree with the other experimental results of Nu_0 placed in an infinite

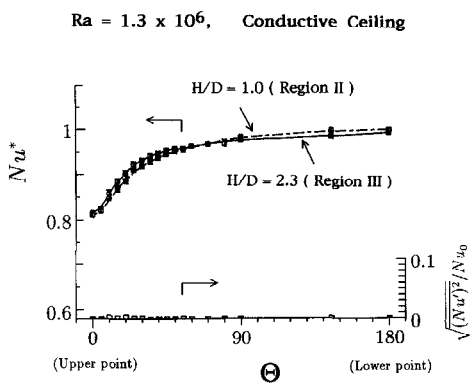

Fig. 5. Nusselt number in region II and III at $Ra = 1.3 \times 10^6$.

fluid medium within the experimental error [1, 8]. We obtain the same results of $Nu^* = 1$ at the lower point of the cylinder in all cases of $H/D = 0.05$, 0.2 (Fig. 4) and 2.3 (Fig. 5). These results are in good agreement with the experiment by Saito *et al.* [1] of the natural convection around a heated horizontal cylinder affected by an upper finite plate, in which the absolute Nusselt number, Nu_0, at the lower point of the cylinder showed almost the same value even when they changed both the width of the upper finite plate and the distance between the cylinder and the upper plate. But Nu^* shows a small amount of change in the region ($90° < \Theta < 180°$) near the lower point of the cylinder as shown in Fig. 4. This result shows that the reduction effect of the velocity along the cylinder by the existence of the ceiling affects the region near the lower point of the cylinder.

3.3. *Evidence of chaotic flow*

Figure 6 shows the cross-correlation of fluid temperature obtained at $Ra = 1.3 \times 10^6$, $H/D = 0.2$ and $\Theta = 0°$ for the case of conductive ceiling. The solid line shows the cross-correlation (the vertical bars showing uncertainty), and the dashed line shows the time-average of fluid temperature. The histogram of its fluctuation intensity is shown at the bottom.

Both the average and the fluctuation intensity are almost uniform in the axial direction of the cylinder, but the cross-correlation decreases rapidly to about 0.35 within $l = 5$ mm. This is due to the unsteady movement of 3D vortices as shown in Fig. 3(b), and then the flow field is considerably three-dimensional and unsteady.

Figure 7 shows the time series of HFS, its power spectra, Liapunov exponents λ_i and Liapunov dimensions D_{KY} in the case of $H/D = 0.2$ and $\Theta = 0°$ at different Rayleigh numbers. Figures 7(a)–(d) are the results for $Ra = 7.4 \times 10^5$, 1.3×10^6, 4.3×10^6 and 1.0×10^7, respectively. The sign $\pm$ in the Liapunov exponents λ_i is calculated from several runs with different parameters τ_{dev}, ε_r, N within the following ranges. The developing time is $3\,\Delta\tau \leqslant \tau_{dev} \leqslant 6\,\Delta\tau$ for sampling time $\Delta\tau = 0.01953$ s. When the extent of the phase space is normalized as unity, the radius of a small ball is $0.03 \leqslant \varepsilon_r \leqslant 0.06$, and the number of the phase points included in it is $10 \leqslant N \leqslant 30$.

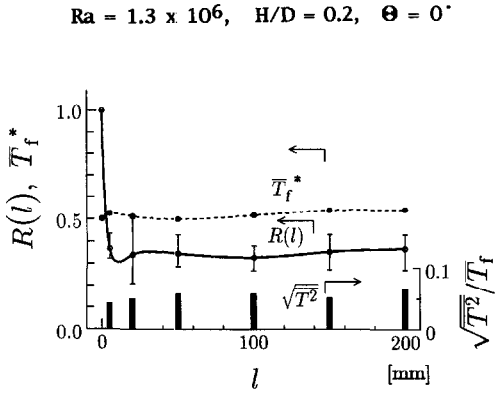

Fig. 6. Cross-correlation.

All power spectra have many peak frequencies which are broadening. For $Ra = 7.4 \times 10^5$ as shown in Fig. 7(a), fluctuation frequencies are below about 1 Hz and its intensity is about 6% [$\sqrt{[(Nu')^2]}/Nu$ (where Nu: local time-averaged value)]. Two positive Liapunov exponents appear and the Liapunov dimension D_{KY} is about 3.3 in the case of $d_m = 4$, 5, 6. Then, the flow can be judged to be chaotic. For $Ra = 1.3 \times 10^6$ as shown in Fig. 7(b), the fluctuation characteristics are almost the same as Fig. 7(a) and its intensity is about 9%. Two positive Liapunov exponents appear and D_{KY} is about 3.5 in the case of $d_m = 4$, 5, 6. For $Ra = 4.3 \times 10^6$ as shown in Fig. 7(c), the fluctuation frequencies are below about 3 Hz and its intensity is about 8%. Two positive Liapunov exponents appear and D_{KY} is about 4.4 in the case of $d_m = 5$, 6. For $Ra = 1.0 \times 10^7$ as shown in Fig. 7(d), fluctuation frequencies are below about 4 Hz and its intensity is about 12%. Three or more positive Liapunov exponents appear and the magnitude of the largest positive Liapunov exponent becomes about twice that of $Ra = 1.3 \times 10^6$, and much higher frequencies 1–4 Hz appear. D_{KY} is about 6.3 in the case of $d_m = 7$, 8.

Figure 8 shows the relation between Liapunov dimension D_{KY} and Rayleigh number Ra for $H/D = 0.2$ which are obtained from the results shown in Fig. 7. From the results of Figs. 7 and 8, we conclude that these unsteady flows around the cylinder affected by the ceiling are rather low-dimensionally chaotic in which their Liapunov dimensions are within about 3–7. Also, we can say that Liapunov dimension increases with Rayleigh number, and much higher frequencies appear in the spectrum with Liapunov dimension going larger.

Figure 9 shows the time-series of TC (TC is placed at $\Theta = 0°$ and $r/D = 1.0$; r is the distance between TC and the cylinder surface), its power spectrum, Liapunov exponents λ_i and Liapunov dimension D_{KY} of the oscillatory flow for $Ra = 1.3 \times 10^6$ and $H/D = 2.3$ in region III of Fig. 2.

The power spectrum has many peak frequencies, which are broadening and below about 3 Hz. The frequency $f = 0.51250$ Hz indicated by an arrow in the figure shows the frequency in which an ascending flow oscillates from side to side. More than two positive Liapunov exponents appear and the largest positive exponent is about twice as much as that of the unsteady flow for $H/D = 0.2$ in region I as shown in Fig. 7(b). Therefore this flow may be strongly chaotic but its dimension could not be obtained by this algorithm, because Liapunov dimension becomes large when the embedding dimension increases.

Noto *et al.* [13, 14] investigated the temperature characteristics of the swaying plume above a line heat source in thermally stable stratified air in an enclosure

Unsteady flow: Conductive ceiling, Region I, H/D = 0.2, HFS, $\Theta = 0^\circ$

(a)

Ra = 7.4 x 10^5

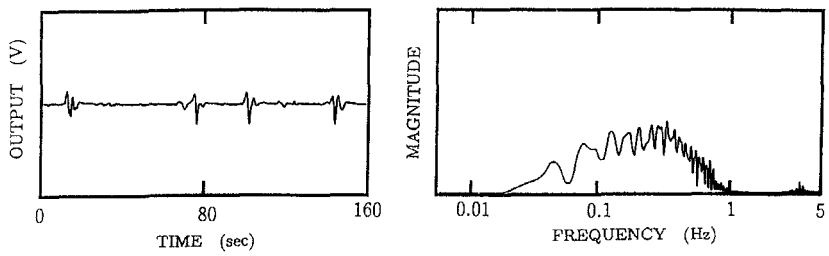

	dm = 4	dm = 5	dm = 6
λ_1	2.6 ± 0.4	2.4 ± 0.4	2.0 ± 0.4
λ_2	1.0 ± 0.3	1.0 ± 0.3	0.6 ± 0.3
λ_3	- 2.0 ± 0.4	- 2.0 ± 0.4	- 1.2 ± 0.3
λ_4	- 8 ± 3	- 5 ± 2	- 4.2 ± 1
λ_5		- 11 ± 3	- 6 ± 2
λ_6			- 12 ± 3
D_{KY}	3.2 ± 0.3	3.3 ± 0.3	3.3 ± 0.3

(b)

Ra = 1.3 x 10^6

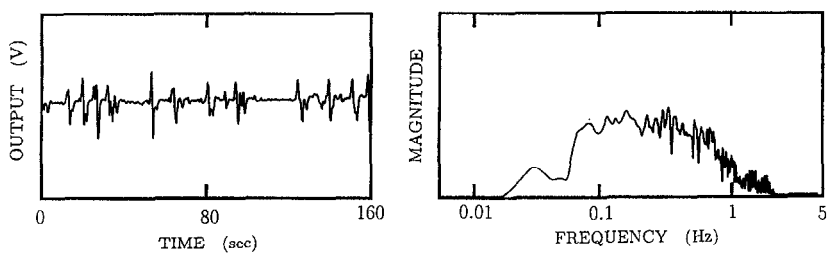

	dm = 4	dm = 5	dm = 6
λ_1	2.9 ± 0.4	2.5 ± 0.4	2.0 ± 0.4
λ_2	0.8 ± 0.3	0.7 ± 0.3	0.6 ± 0.3
λ_3	- 1.3 ± 0.3	- 1.2 ± 0.3	- 1.0 ± 0.4
λ_4	- 6 ± 2	- 4.2 ± 1	- 3.2 ± 0.5
λ_5		- 10 ± 3	- 7 ± 2
λ_6			- 13 ± 3
D_{KY}	3.4 ± 0.3	3.5 ± 0.3	3.5 ± 0.3

Fig. 7. Characteristics of unsteady flow in region I: (a) $Ra = 7.4 \times 10^5$; (b) $Ra = 1.3 \times 10^6$; (c) $Ra = 4.3 \times 10^6$ and (d) $Ra = 1.0 \times 10^7$.

Ra = 4.3 x 10^6

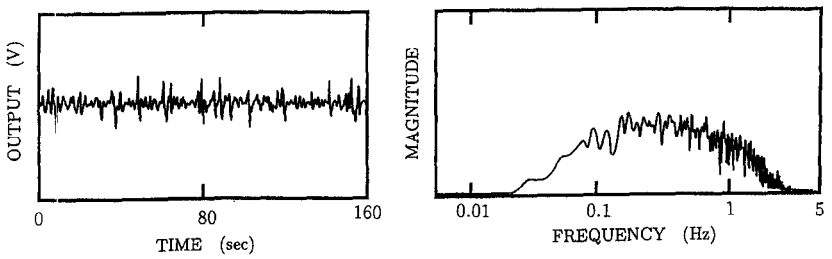

	dm = 5	dm = 6
λ_1	4.4 ± 0.8	3.8 ± 0.6
λ_2	2.1 ± 0.4	1.6 ± 0.4
λ_3	- 0.3 ± 0.3	- 0.3 ± 0.3
λ_4	- 3.6 ± 0.5	- 2.6 ± 0.4
λ_5	- 10 ± 3	- 6 ± 1
λ_6		- 13 ± 3
D_{KY}	4.3 ± 0.3	4.4 ± 0.3

(c)

Ra = 1.0 x 10^7

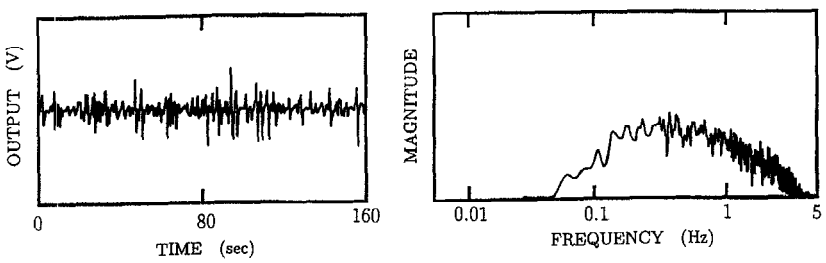

(d)

	dm = 7	dm = 8
λ_1	6.6 ± 0.8	6.0 ± 0.8
λ_2	4.3 ± 0.5	4.0 ± 0.4
λ_3	1.7 ± 0.5	2.1 ± 0.5
λ_4	- 0.2 ± 0.4	0.3 ± 0.4
λ_5	- 2.6 ± 0.5	- 1.5 ± 0.7
λ_6	- 6 ± 1	- 4.3 ± 0.6
λ_7	- 14 ± 1	- 8 ± 1
λ_8		- 15 ± 1
D_{KY}	6.3 ± 0.5	6.3 ± 0.5

Fig. 7—*Continued.*

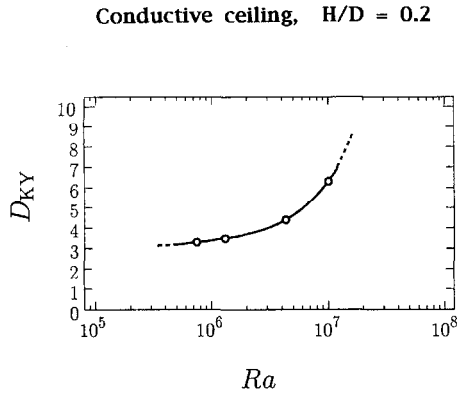

Fig. 8. Relation between Liapunov dimension and Rayleigh number.

to clarify the transition performance of the plume to turbulence by analyzing the time-series obtained from the sensor. Igarashi [15] investigated the condition of generating the oscillatory flow above a line heat source placed in the horizontal rectangular duct with various aspect ratio. Such an unstable flow was investigated for $H/D \sim \infty$ and $Ra < 10^2$. We investigated the unstable flow characteristics such as the unsteady flow in region I and the oscillatory flow in region III from the standpoint of chaos for $H/D \leqslant 2.3$ and Rayleigh numbers ranging from 4.8×10^4 to 1.0×10^7.

4. CONCLUSION

In order to clarify the flow and heat transfer performance around an isothermally heated horizontal cylinder affected by the flat ceiling, the experiment was performed for different distances between the ceiling and the cylinder under two temperature conditions of the ceiling (conductive and adiabatic) at Rayleigh numbers ranging from 4.8×10^4 to 1.0×10^7.

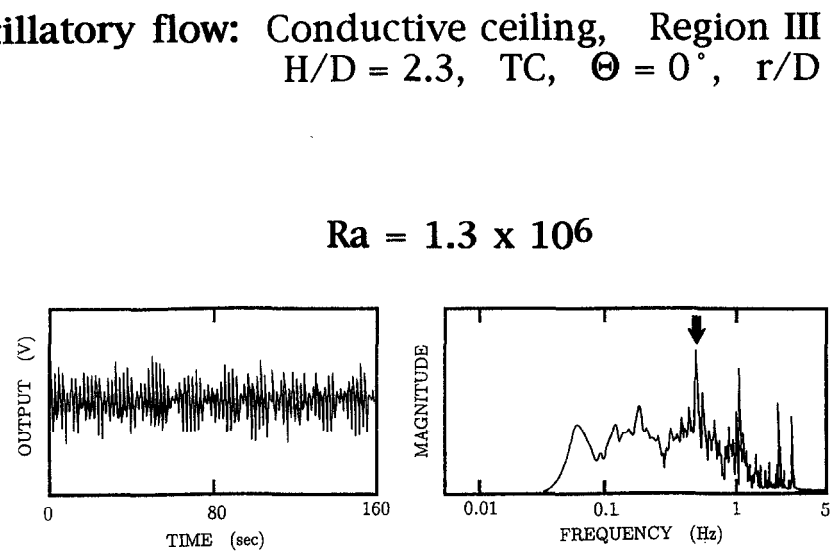

	dm = 5	dm = 6	dm = 7	dm = 8
λ_1	5.5 ± 1.0	7.6 ± 1.5	8.5 ± 0.5	11.5 ± 1.5
λ_2	2.6 ± 0.6	4.1 ± 0.6	4.1 ± 1.0	6.1 ± 1.5
λ_3	0.0 ± 0.4	1.3 ± 0.4	1.3 ± 0.5	3.3 ± 0.8
λ_4	- 3.4 ± 0.5	- 1.5 ± 0.4	- 1.5 ± 0.4	1.2 ± 0.6
λ_5	- 10 ± 3	- 5 ± 2	- 4 ± 1	- 0.5 ± 0.5
λ_6		- 13 ± 3	- 5 ± 1	- 3 ± 1
λ_7			- 13 ± 2	- 6 ± 1
λ_8				- 14 ± 2
D_{KY}	4.5 ± 0.3	5.5 ± 0.3	6.6 ± 0.3	7.8 ± 0.4

Fig. 9. Characteristics of oscillatory flow in region III.

The conclusions obtained are as follows:

(1) Three types of flow patterns are observed for the case of conductive ceiling depending on Rayleigh number Ra and dimensionless distance H/D between the ceiling and the cylinder: 3D unsteady flow in which the flow along the cylinder separates on its upper surface, 2D steady flow, and oscillatory flow.

(2) For $Ra = 1.3 \times 10^6$ and $H/D = 0.05$ in region I of Fig. 2, the flow around the cylinder for the conductive ceiling are unsteady and 3D, but for the adiabatic ceiling the flow is stable and scarcely shows fluctuation. That is, the instantaneous and time-averaged heat transfer performances around the cylinder for both conductive and adiabatic ceilings are extremely different.

(3) The unsteady flow of $H/D = 0.2$ in region I of Fig. 2 for the conductive ceiling is 3D. Two or more positive Liapunov exponents appear and their Liapunov dimensions are within about 3–7, therefore these flows are shown to be chaotic. Furthermore, we clarify that the Liapunov dimension increases with the Rayleigh number, and much higher frequencies appear in the spectrum with the Liapunov dimension larger.

(4) The oscillatory flow in which an ascending flow begins to oscillate from the intermediate region between the ceiling and the cylinder in region III of Fig. 2 is 3D and chaotic.

Acknowledgement—The authors are grateful to Mr Hironori Miyoshi, graduate student of the University of Electro-Communications, for his experimental performance throughout this work.

REFERENCES

1. T. Saito, R. Ishiguro and Y. Fujishima, Natural convection heat transfer around a horizontal cylinder (effect of the horizontal plate placed upper the cylinder), *Proceedings of the 6th National Heat Transfer Symposium of Japan* (in Japanese), pp. 61–64 (1969).
2. C. D. Jones and D. J. Masson, An interferometric study of free convection heat transfer from enclosed isothermal surfaces, *Trans. ASME* **77,** 1275–1281 (1955).
3. R. E. Powe, C. T. Carley and E. H. Bishop, Free convective flow patterns in cylindrical annuli, *J. Heat Transfer* **91,** 310–314 (1969).
4. Y. Takata, K. Iwashige, K. Fukuda and S. Hasegawa, Three-dimensional natural convection in an inclined cylindrical annulus, *Int. J. Heat Mass Transfer* **27,** 747–753 (1984).
5. Y. F. Rao, Y. Miki, Y. Takata and S. Hasegawa, Flow patterns of natural convection in horizontal cylindrical annuli, *Int. J. Heat Mass Transfer* **28,** 705–714 (1985).
6. M. Steinberg, H. C. Cheng and F. Horn, A system study for the removal, recovery and disposal of carbon dioxide from fossil fuel power plants in the U.S., Report of Brookhaven National Laboratory, RNL-35666 (1984).
7. H. Ishitani, R. Matsuhashi, S. Oomura, S. Shimada and T. Suyari, Feasibility study on CO_2 disposal in the ocean, *Energy Resources* (in Japanese) **12,** 296–304 (1991).
8. T. H. Kuehn and R. J. Goldstein, Numerical solution to the Navier–Stokes equations for laminar natural convection about a horizontal isothermal circular cylinder, *Int. J. Heat Mass Transfer* **23,** 971–979 (1980).
9. M. Sano and Y. Sawada, Measurement of the Lyapunov spectrum from a chaotic time series, *Phys. Rev. Lett.* **55,** 1082–1085 (1985).
10. H. Nagashima and Y. Baba, *Chaos* (in Japanese). Baifukan, Tokyo (1992).
11. H. Koizumi and I. Hosokawa, Unsteady behavior and mass transfer performance of the combined convective flow in a horizontal rectangular duct heated from below, *Int. J. Heat Mass Transfer* **36,** 3937–3947 (1993).
12. S. Chandrasekhar, *Hydrodynamic and Hydromagnetic Stability*. Clarendon Press, Oxford (1961).
13. K. Noto, S. Maeda and T. Nakajima, Temperature characteristics of the swaying plume above a line heat source in thermally stable stratified air, *Trans. JSME* (in Japanese) *Ser. B* **58,** 3421–3428 (1992).
14. K. Noto, K. Tsutsui and T. Nakajima, Plume pattern with swaying motion amplified by thermally stable stratification, *Trans. JSME* (in Japanese) *Ser. B* **58,** 3429–3436 (1992).
15. T. Igarashi, Oscillatory phenomena of natural convection in an enclosure (line heat source in the horizontal rectangular duct), *Trans. JSME* (in Japanese) *Ser. B* **43,** 3839–3847 (1977).